

Numerical simulations on adiabatic shear behaviour of 921A steel pure shear hat-shaped specimens

J. C. Li, X. W. Chen & G. Chen
*Institute of Structural Mechanics,
China Academy of Engineering Physics, China*

Abstract

The adiabatic shear behaviour of a specimen is observed, based on a series of numerical simulations of SHPB test using 921A steel pure shear hat-shaped specimens in the present paper. The initiation and the propagation of an adiabatic shear band (ASB) and the relative distribution of temperature field in the specimen are analyzed. It is found that ASB is formed as the spread of an unstable zone with high temperature and high strain in the two ends of the Shear Zone. The spread speed of an ASB is related to the loading rate V_0 , whilst the width of ASB is nearly independent of the loading rate. All the ASBs are deformed bands corresponding to various values of V_0 .

Keywords: SHPB, pure shear hat-shaped specimen, adiabatic shear deformation, numerical simulation.

1 Introduction

Adiabatic shear deformation usually occurs in the high-speed deformations such as high-speed impact and penetration, etc. Adiabatic rising-temperature will lead the thermal softening effect and thus adiabatic shear band (ASB) occurs in the material. An ASB usually has a width of 10–100 μm , in which the shear strain, shear strain rate and temperature can achieve a value of 1–10², 10⁵–10⁷s⁻¹, and 10²–10³K, respectively.

Meyers et al. [1] designed a pure shear hat-shaped specimen as shown in Figure 1, in which the Shear Zone deforms as a pure shear deformation when the specimen undergoes compressive loading. This hat-shaped structure has been used widely to study the adiabatic shear behaviour of material. Accompanied



with the development of computer techniques, numerical simulation method becomes more and more important in the researches on adiabatic shear deformation and numerous relative simulations have been conducted, of which, the outstanding work is Batra and his colleagues'. Moreover, previous researches on adiabatic shear deformation are mainly based on stress / strain field.

The adiabatic shear behaviour of material affects directly its performance under high strain rates. Chen et al. [2] conducted SHPB tests and corresponding simulations using 921A steel pure shear hat-shaped specimens and found that, while under a comparatively high loading rate, the large-deformation zone in the specimen centralizes gradually to the designed Shear Zone, and fracture occurs in the Shear Zone with increasing the loading rate to a certain value.

In general, the deformation process of specimen can't be observed in detail in SHPB test; furthermore, it is hard to conduct SHPB test under an ultrahigh loading rate. However, it becomes possible to conduct SHPB test under an ultrahigh loading rate in numerical simulation; also, the history of deformation and failure of the specimen can be observed conveniently. In the present paper, integrated with Chen et al. [2]'s tests, a series of numerical simulations of SHPB test using 921A steel pure shear hat-shaped specimens are conducted with ANSYS/LS-DYNA, and the adiabatic shear behaviour of specimen is observed.

2 FEM model

All the bars in Chen et al. [2]'s tests are made of alloy steel, and the geometry of 921A steel pure shear hat-shaped specimen is shown in Figure 1.

Firstly, a numerical test is conducted with ANSYS/LS-DYNA to replay the SHPB test done by Chen et al. [2]. Regarding its axial symmetry, an axial symmetric FEM model is employed in the numerical simulation and all the elements are defined as shell-162 axial symmetric elements. Especially, the meshes of the Shear Zone are fined to adapt the simulation, and the minimum mesh size of the Shear Zone is modified as about $30\mu\text{m}$. As the width of ASB usually doesn't exceed $100\mu\text{m}$, and the characteristic size of a crystal is 10–60 μm , thus the meshes could satisfy the relative requirement of simulation.

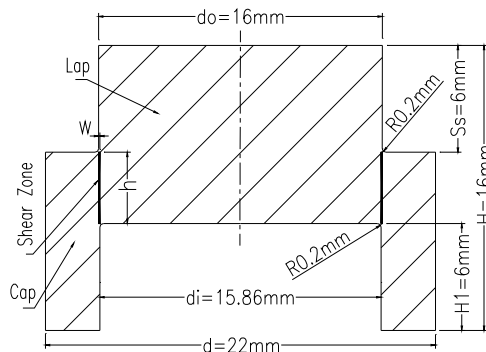


Figure 1: Geometry of a 921A steel pure shear hat-shaped specimen.

The deformation is adiabatic and thus heat exchange is neglected in the simulations. The material of all bars is defined as isotropic elastic, and the specimen is described by Johnson-Cook model (Johnson and Cook [3]) and Gunnison EOS for simulating its adiabatic shear deformation well. Johnson-Cook model includes both the definitions of flow stress and fracture strain of material, and in its fracture model accumulative damage is used to analyze the failure of material. Based on Chen et al. [2]'s tests, the largest fracture strain is used as the criterion of element erosion and its value is defined as 1.13. Element is deleted immediately when it erodes. In general, it is assumed that 90 per cent of the deformation energy of material transforms into heat energy, and the rest transforms into strain energy of material, thus the temperature rising in material could be calculated from the increase of stress and strain using the dependence of $dT=0.9\sigma d\varepsilon/(\rho C_p)$, where ρ is the density of material and C_p the specific thermal capacity. Corresponding specimen material parameters are listed in Table 1.

Table 1: Specimen material parameters of Johnson-Cook model.

ρ (kg/m ³)	G (GPa)	E (GPa)	ν	C_p (J/(kg•k))	T_r (k)
7800	0.7776	205	0.28	400.90	300
T_m (k)	A (MPa)	B (MPa)	C	n	m
1765	760	500	0.014	0.53	1.13
D_1	D_2	D_3	D_4	D_5	
1.13	0	0	0	0	

Regarding the same loading conditions, same strain waves and deformations of specimen as that of Chen et al. [2] are obtained in numerical simulations, thus the validation of the numerical model is confirmed. Then simulations under different loading rates are conducted using the same model. Detailed data of simulation model, strain waves and deformations of specimen can be seen in previous paper of the authors in DYMAT2009 (Li et al. [4]).

3 Adiabatic shear deformations of the specimens

Numerical simulations of SHPB test under different loading rates are conducted by using the method mentioned above. Different strain waves in the bars and dynamic deformations of the specimens under different loading rates V_0 are obtained (seen in [4]). Here only the adiabatic shear behaviours of the specimens will mainly be discussed.

Wright and Batra [5] conducted one-dimensional simulations of adiabatic shear deformation and found the phenomenon of stress collapse, i.e. the stress in an ASB keeps almost invariable for a certain period while it approaches to the largest value, and then descends rapidly. Wright and Ockendon [6] further analyzed stress collapse basing on asymptotic analysis method and suggested three criteria of the initiation of ASB, i.e. the effective plastic strain reaches 0.5, effective stress reaches the largest value or stress collapse occurs, respectively. Analysis on adiabatic shear deformation will be conducted integrated with these three criteria in this paper.



As adiabatic shear deformation occurs mainly in the Shear Zone, only the deformation of Shear Zone and its surrounding regions is emphatically observed. Corresponding analytical zone is shown in Figure 2, where X-coordinate represents the distance from the central symmetrical axis, and Y-coordinate the distance from the bottom of the Cap. Five elements in different locations of the Shear Zone are selected as the characteristic analytical elements, and they are marked as 22832, 22306, 22300, 22293 and 23238, respectively, from the top of the Shear Zone to its bottom. In Figure 2, the Y-coordinate value of the transverse zone denoted by broken line is 8, and the X-coordinate value of the longitudinal zone denoted by dash-dotted line is also 8. Moreover, the transverse zone intersects with the longitudinal zone in element 22300 which locates in the centre of Shear Zone.

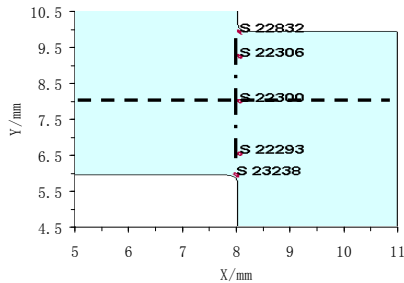


Figure 2: The analytical zone.

3.1 Histories of stress and strain in the Shear Zone

According to the criteria of the initiation of ASB in [6], whether adiabatic shear deformation has occurred could be identified based on the histories of the stress and strain in the Shear Zone. Histories of effective stress in element 22300 under different loading rates V_0 are shown in Figure 3, where only the period in which the effective stress varies obviously is shown for the clarity of figure.

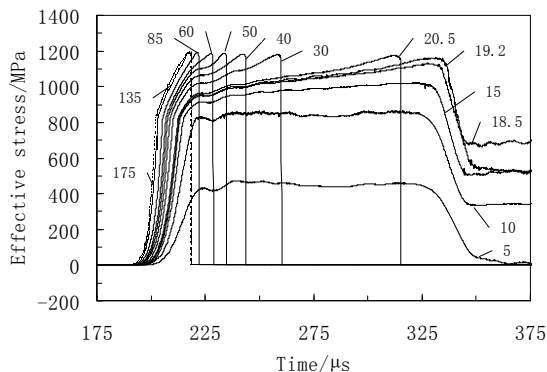


Figure 3: Histories of effective stress in element 22300 under different V_0 s (m/s).

From Figure 3 it can be seen that within the loading rate range of $V_0 < 19.2\text{m/s}$, effective stress in element 22300 doesn't reach its largest value, and lower loading rate corresponds to smaller effective stress. Stress collapse doesn't occur in the element, and the decline of stress in the end of pulse is due to the unloading of extra load; when $V_0 = 19.2\text{m/s}$, effective stress approaches to the largest value and stress collapse occurs; while $V_0 \geq 20.5\text{m/s}$, the Shear Zone finally fractures thoroughly, and effective stress declines immediately to zero when it reaches the largest value because of the element erosion. Moreover, as V_0 increases, both the time that effective stress reaches its largest value and the initiation time of element erosion move up gradually.

Correspondingly, it can be found from the histories of effective plastic strain in element 22300 that, when $V_0 = 5\text{m/s}$, there is no plastic strain because the specimen is still elastic; while $V_0 \geq 10\text{m/s}$, plastic deformation initiates in the element. However, within the range of $V_0 < 19.2\text{m/s}$, the value of effective plastic strain is less than 0.5, and lower loading rate corresponds to smaller effective plastic strain. When $V_0 = 19.2\text{m/s}$, effective plastic strain exceeds 0.5. Regarding higher loading rates, effective plastic strain declines immediately to zero when it reaches the critical value of fracture strain because of the erosion of element. Moreover, histories of effective plastic strain in the element are consistent with that of effective stress, i.e. same conclusions for the analysis of adiabatic shear deformation could be obtained from either effective stress or effective plastic strain, and latter analysis in this paper is mainly based on the effective plastic strain.

It can also be found from Figure 3 that while the loading rate is comparatively low (e.g. $V_0 = 18.5\text{m/s}$), ASB may occurs in its two ends although adiabatic shear deformation does not initiate in the centre of Shear Zone. Therein it needs to analyze the histories of effective plastic strain in the ends of Shear Zone. Not losing the universality, elements 22306, 22293 are selected as the example, and the histories of effective plastic strain in these two elements under comparatively low loading rates are shown in Figure 4.

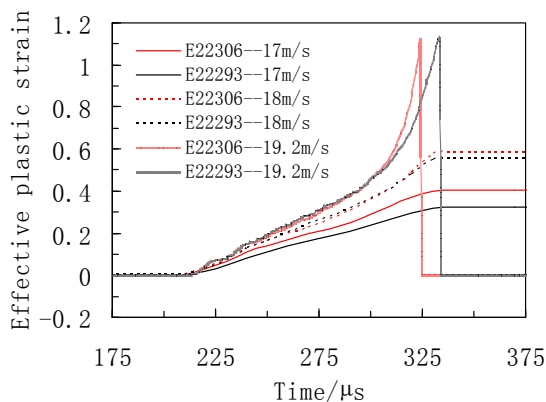


Figure 4: Histories of effective plastic strain in the elements in the ends of Shear Zone under different V_0 s.

It can be seen from Figure 4 that when $V_0=17\text{m/s}$, all the effective plastic strain doesn't reach the value of 0.5; however, when $V_0=18\text{m/s}$, effective plastic strain exceeds 0.5; and when $V_0=19.2\text{m/s}$, both elements erode and effective plastic strain declines to zero correspondingly. Thus, it can be known that, within the range of $V_0 < 18\text{m/s}$, adiabatic shear deformation has not occurred in the specimen; while $V_0 \geq 18\text{m/s}$, ASB initiates in the two ends of Shear Zone, however, fracture doesn't occur in the specimen; when $V_0=19.2\text{m/s}$, ASB runs through all the Shear Zone, and adiabatic shear fracture begins to initiate in its two ends; while $V_0 \geq 20.5\text{m/s}$, all the ASB fractures thoroughly.

Moreover, it can also be found from the histories of effective plastic strain ε_p that, the initiation of ASB in the Shear Zone becomes earlier and earlier with increasing the loading rate. Besides, the duration from $\varepsilon_p=0.5$ to element erosion becomes shorter and shorter, i.e. the carrying capacity of specimen trails off gradually with increasing the loading rate. Here element 22832 which locates in the top of Shear Zone, is selected as an example to analyze the variety of ASB initiation and element erosion with increasing the loading rate, and the elements in the Shear Zone are all similar to it. Initiation time of $\varepsilon_p=0.5$ and element erosion of element 22832 versus loading rates are shown in Figure 5, the interval between these two time is defined as the duration from the initiation of ASB to element erosion.

It can be seen from Figure 5 that, both the initiation time of ASB and element erosion move up with increasing the loading rate. While the loading rate is comparatively low ($V_0 < 40\text{m/s}$), both the initiation time of ASB and element erosion move up distinctly; however, while $V_0 \geq 40\text{m/s}$, the trend of moving up of the initiation time slows down rapidly, and then the time approaches to a saturated value.

Moreover, from Figure 5 it can also be known that the duration from the initiation of ASB to element erosion shortens obviously with increasing the loading rate, and gradually approaches to a saturated value, i.e. $2\mu\text{s}$, after $V_0 \geq 40\text{m/s}$. It indicates that the carrying capacity of specimen trails off with increasing the loading rate and approaches to its lower limit.

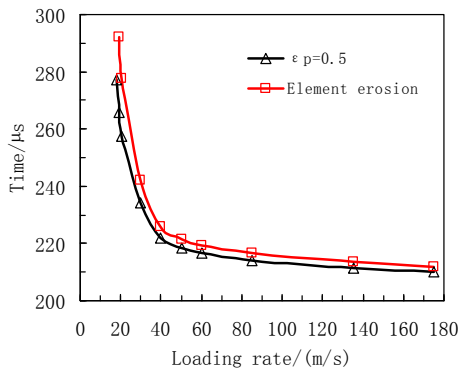


Figure 5: Initiation time of $\varepsilon_p=0.5$ and element erosion of element 22832 versus loading rates.

3.2 History of rising-temperature in the specimen

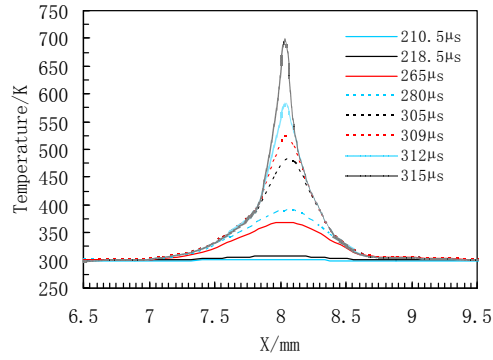
In this section the rising-temperature in specimen will be discussed. According to the deformations of specimen in the simulations [4], the case of $V_0=20.5\text{m/s}$ is selected as an example, and the transverse zone and longitudinal zone shown in Figure 2 are mainly observed. Temperature distribution of the analytical zone is shown in Figure 6, where (a) is temperature curve of the transverse zone and (b) that of the longitudinal zone, in which the eroded elements are no longer shown.

From Figure 6(a) it can be seen that when the specimen deforms under $V_0=20.5\text{m/s}$, temperature rising in the transverse zone mainly centralizes in a narrow band which consists of the Shear Zone and its surrounding regions ($7.5\text{mm} < X < 8.5\text{mm}$). Before the time $t=210.5\mu\text{s}$, no obvious temperature rising occurs in the specimen; then temperature in the Shear Zone and its surrounding regions begins to rise; before $t=280\mu\text{s}$, temperature in the zone within a distance of 0.5mm from the centre of Shear Zone rises continuously, and temperature rising in the Shear Zone is faster than that in its surrounding regions. A gauss distribution of temperature is formed. After $t=280\mu\text{s}$, temperature in the Shear Zone rises rapidly and reaches about 700K when the element erodes, whereas temperature in the surrounding regions almost no longer change. Furthermore, in the whole process of deformation, there is no obvious temperature rising in the regions out the distance of 0.5mm from the Shear Zone. Thus, the deformation of specimen confirms the qualification of adiabatic shear deformation well.

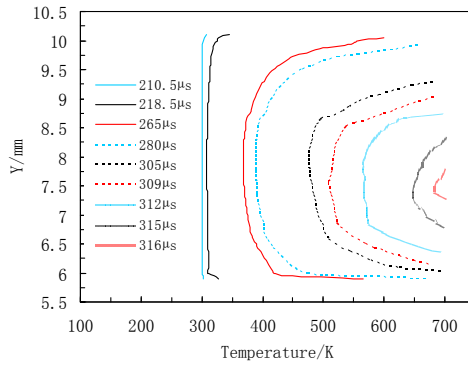
Correspondingly, it can be found from Figures 6 (b, c) that, when $t=210.5\mu\text{s}$, temperature rising initiates in the two ends of Shear Zone, then the zone with temperature rising extends towards the inner regions of Shear Zone. When $t=218.5\mu\text{s}$ obvious temperature rising occurs in the whole Shear Zone, and subsequently the zone with temperature rising extends transversely and becomes wider. When $t=280\mu\text{s}$ shear fracture occurs in the two ends of Shear Zone, and the transverse extension of the zone with temperature rising stops. When the two ends of Shear Zone fractures, its temperature rises rapidly to about 700K . The shear fracture follows to evolve towards the inner region of Shear Zone, and especially, a small zone with lower temperature of about 600K forms in the tip of the crack. With the evolution of adiabatic shear fracture and the spread of the high-temperature zone, temperature in the whole Shear Zone rises rapidly. At this time, the distribution of temperature in the Shear Zone behaves as higher in the two ends and lower in the inner. Moreover, the width of high-temperature zone almost doesn't change in the whole process of deformation.

Within the loading rate range of $V_0 < 85\text{m/s}$, the deformation of specimen is similar to that of the case $V_0=20.5\text{m/s}$. Corresponding to different loading rates, the fracture in specimen always extends from the two ends of Shear Zone to its centre. Besides, material temperature always rises to about 700K before it fractures. However, with increasing the loading rate, the initiation time of temperature rising in specimen moves up quickly, and the initiation of shear fracture in the Shear Zone becomes earlier. Also the duration of shear fracture shortens rapidly. Moreover, within this loading rate range, the width of the temperature-rising zone is almost the same as that at loading rate $V_0=20.5\text{m/s}$.

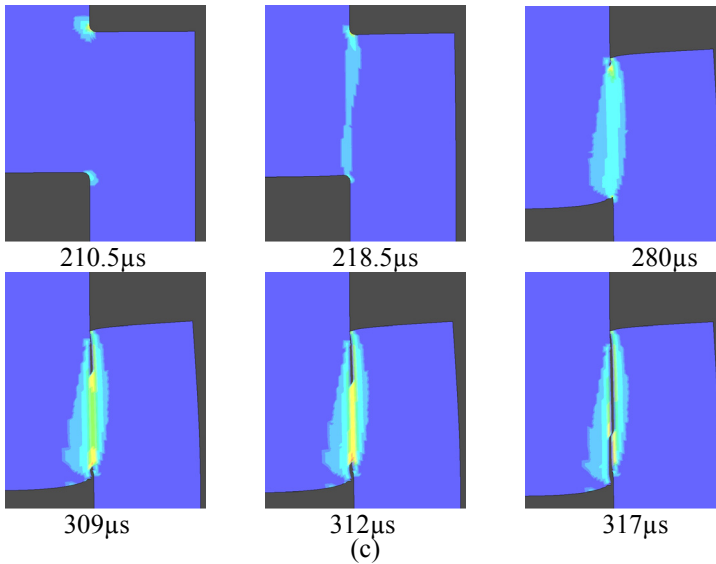




(a)



(b)



(c)

Figure 6: Temperature distribution and deformation evolution of the analytical zone under $V_0=20.5\text{m/s}$.

When V_0 exceeds 85m/s, the Cap of specimen yields and becomes stub before the fracture of Shear Zone (seen in [4]), also the stub Cap compresses the Lap transversely. Before the initiation of ASB, the temperature rising in the Shear Zone and its surrounding regions is higher than that under loading rates of $V_0 < 85\text{m/s}$, and temperature of the Cap also rises rapidly because of its intense plastic deformation. Therein the zone with high temperature is a little wider than that under loading rates of $V_0 < 85\text{m/s}$.

3.3 Distributions of stress, strain and temperature in the tip of ASB

Kuriyama and Meyers [7] predicted that there is an unstable zone with a width of about $5\mu\text{m}$, high strain and comparatively low stress in the tip of ASB, and ASB extends following it. Figures 6(b, c) show that ASB in the specimen is formed due to the spread of a high-temperature zone from the ends of Shear Zone towards its centre. Thereinafter the distributions and evolutions of stress, strain and temperature in the tip of shear crack will be analyzed in detail.

The case of $V_0 = 60\text{m/s}$ is selected as an example, and the contours of effective stress σ_{eff} , effective plastic strain ϵ_p and temperature T around the crack tip of Shear Zone at $t = 225.5\mu\text{s}$ are shown in Figure 7. From the figure it can be seen that the effective stress, effective plastic strain and temperature in the Shear Zone are all abruptly higher than that in other regions of the specimen. In the tip of the shear crack there assuredly exists a small zone with higher effective plastic strain and higher temperature than that in other parts of the Shear Zone, and the characteristic scale of this small zone is almost the same as the size of meshes ($\sim 30\mu\text{m}$). However, there is no obvious difference of the effective stress in the Shear Zone. Moreover, simulations show that before the initiation of fracture in the specimen, effective plastic strain in the two ends of Shear Zone is already obviously higher than that in other regions. After the shear fracture initiates, a small zone with higher temperature and higher effective plastic strain always exists in the front of the shear crack until the Shear Zone fractures thoroughly. The smallest mesh in the simulations is about $30\mu\text{m}$, which is far larger than $5\mu\text{m}$, and thus it may be too large to show the lower stress zone in the tip of the shear crack. However, ASB forms following the spread of the unstable zone with higher temperature and higher strain in the front of the shear crack, which are absolutely consistent with Kuriyama and Meyers [7].

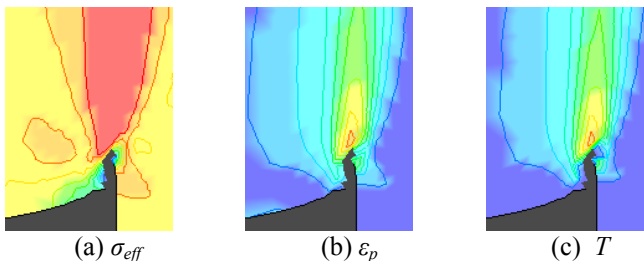


Figure 7: Contours of effective stress, effective plastic strain and temperature in the Shear Zone in case of $V_0 = 60\text{m/s}$ and $t = 225.5\mu\text{s}$.

3.4 Spread speeds of ASB and fracture

According to the analysis in Section 3.1, the duration of fracture in the Shear Zone shortens with increasing the loading rate, and also the element erodes rapidly after the initiation of ASB as shown in Figure 5. Therein the spread speed of ASB in the Shear Zone increases with increasing the loading rate. Supposing the time of $\varepsilon_p = 0.5$ in elements 22832 and 22300, as shown in Figure 2, as the instant initiation of ASB in the end of Shear Zone, and that the ASB runs through all the Shear Zone, respectively, and thus the interval between these two instant time is the duration of ASB spreading in the Shear Zone. Likewise, the time interval between the erosion of these two elements is the duration of spread of fracture in the Shear Zone. Thus the average spread speeds of ASB and element erosion versus the loading rates could be calculated integrated with the length of Shear Zone, respectively, as shown in Figure 8.

Figure 8 shows that both the average speeds increase with increasing the loading rate, and the increase of spread speed of element erosion is quicker than that of ASB. Corresponding to comparatively high loading rates, the average spread speeds of ASB and element erosion approaches to a saturated value of 200m/s and 235m/s, respectively. There exists two phases in the spread of ASB according to Lebouvier and Lipinski [8], i.e., the spread speed of ASB depends linearly and intensively on the loading rate when the loading rate is comparatively low, while under a higher loading rate, the spread speed of ASB increases little and approaches to a saturated value. Figure 8 consists with Lebouvier and Lipinski [8] well.

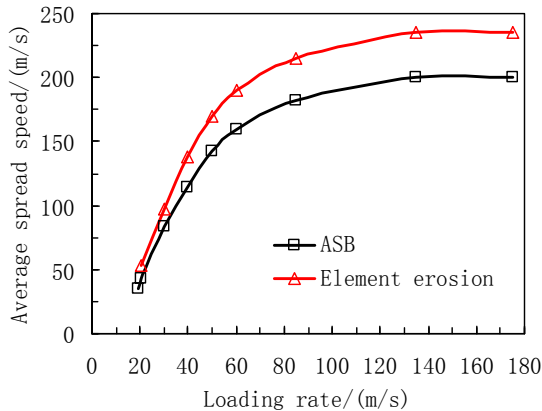


Figure 8: Average spread speeds of ASB and element erosion vs loading rates.

3.5 The width of ASB and its type

This section discusses the dependence of the width of ASB on the loading rate. The temperature distributions of the transverse analytical zone at the initiation of erosion of element 22300 under different loading rates are shown in Figure 9.

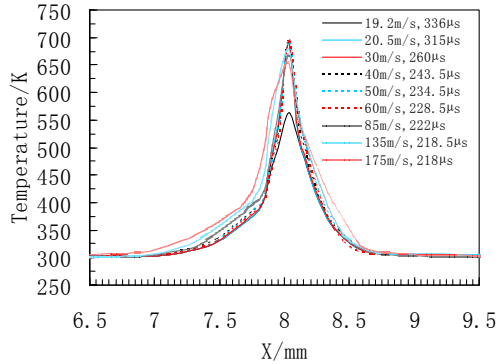


Figure 9: Temperature distributions of the transverse analytical zone at time of erosion initiation of element 22300 under different loading rates.

When $V_0=19.2\text{m/s}$, because the bars stop to compress the specimen after the shear fracture occurs in the ends of Shear Zone, the temperature of element 22300 only reaches about 550K and no longer rises up; while if $V_0 \geq 20.5\text{m/s}$, temperature of the element always rises rapidly to about 700K before it erodes. Besides, in the loading rate range of $20.5\text{m/s} < V_0 < 85\text{m/s}$, the width of the high temperature zone is almost the same. Integrated with the temperature distributions and the specimen deformations, it can be found that the width of ASB is about $70\mu\text{m}$ and it approximates to the width of Shear Zone.

However, while if $V_0 \geq 85\text{m/s}$, the Cap of specimen becomes stub (seen in [4]), and severe plastic deformation of the Cap leads the obvious temperature rising in specimen rather than the Shear Zone, and thus the zone with high temperature becomes wider. Essentially in that case, the deformation of specimen no longer satisfies the condition of pure shear, so the enlargement of high-temperature zone doesn't mean that the ASB becomes wider. Therein the width of ASB in the specimen is almost independent of the loading rate.

In general, it is supposed that when temperature achieves a value of $T=0.4T_m$, where T_m is the melting temperature of metal material, a second crystallization will occur in the material and the ASB will transform to a transformed band from deformed band. In other words, if $T < 0.4T_m$, the corresponding ASB is a deformed band. The melting temperature of 921A steel is 1765K, and $0.4T_m = 706\text{K}$ correspondingly. Regarding all of the loading rates in the simulations, the maximum temperature in ASB is always less than 706K, thus it can be concluded that transformed band never occurs in the hat-shaped specimen during its deformation process, i.e. corresponding ASBs are all deformed bands.

4 Conclusions

Integrated with relative tests, the adiabatic shear behaviour of 921A steel pure shear hat-shaped specimen is analyzed by means of the numerical SHPB tests.



When the specimen is compressed, the temperature rising mainly centralizes in the Shear Zone. If the loading rate is comparatively low ($V_0 < 18$ m/s), adiabatic shear deformation doesn't occur in the specimen; while if $V_0 \geq 18$ m/s, ASB begins to initiate in the two ends of Shear Zone. When V_0 increases to 19.2 m/s, adiabatic shear deformation has run through all the Shear Zone; especially if $V_0 \geq 20.5$ m/s, the Shear Zone fractures thoroughly because of adiabatic shear deformation. ASB always develops from the two ends of Shear Zone to its centre. There is a small unstable zone with higher temperature and higher strain in the tip of shear crack, and it extends towards the centre of Shear Zone along with the evolution of fracture.

Moreover, both average spread speeds of ASB and fracture increase with increasing the loading rate, and approach to a respective saturated value. Besides, the spread speed of fracture is higher than that of ASB. The width of ASB is little dependent on the loading rate and equals to about $70\mu\text{m}$, which approximates to the width of Shear Zone. All ASBs corresponding to various loading rates in this paper are deformed bands.

References

- [1] Meyers, M.A., Meyer, L.W., Beatty, J., et al. High strain, high strain-rate deformation of copper. *Proc. of "Shock waves and high-strain-rate phenomena in materials"*, eds. M.A. Meyers, L.E. Murr, K.P. Staudhammer and M. Dekker. USA: New York, pp. 529-542, 1992.
- [2] Chen, G., Chen, X.W., Pan, X.X., et al. Numerical simulation and experiments on the dynamic deformation of 921A steel hat-specimen. *Transactions of Beijing Institute of Technology*, 29(Suppl. 1), pp. 106-110, 2009. (in Chinese)
- [3] Johnson, G.R., Cook, W.H. A constitutive model and data for metals subjected to large strains, high strain rates and high temperatures. *Proc. of the 7th International Symposium on Ballistics*. Netherlands: The Hague, pp. 541-552, 1983.
- [4] Li, J.C., Chen, X.W., Chen, G. Numerical simulations of SHPB test using 921A steel pure shear hat-shaped specimens. *Proc. of 9th International Conference on the Mechanical and Physical Behaviour of Materials under Dynamic Loading (DYMAT 2009)*. Brussels, Belgium, pp.1685-1692, Sept. 7-11, 2009.
- [5] Wright, T.W., Batra, R.C. The initiation and growth of adiabatic shear bands. *Int J Plasticity*, 1, pp. 205-212, 1985.
- [6] Wright, T.W., Ockendon, H. A model for fully formed shear bands. *J Mech Phys Solids*, 40(6), pp. 1217-1226, 1992.
- [7] Kuriyama, S., Meyers, M.A. Numerical modeling of the propagation of an adiabatic shear band. *Metallurgical Trans A*, 17A, pp. 443-449, 1986.
- [8] Lebouvier, A.S., Lipinski, P. Numerical study of the propagation of an adiabatic band. *J Phys IV France*, 10, pp. 403-408, 2000.

